CHALMERS
UNIVERSITY OF TECHNOLOGY

An all-in-one multifunctional carbon fiber composite material using electrochemistry

Materials Today 98 (2026) 103422

Contents lists available at ScienceDirect

Materials Today

journal homepage: www.elsevier.com/locate/mattod

An all-in-one multifunctional carbon fiber composite material using electrochemistry

Alfredo Bici [a], Elvira Lind [b], Richa Chaudhary [c], Leif E. Asp [c], Göran Lindbergh [b], Dan Zenkert [a,*]

[a] Department of Engineering Mechanics, KTH Royal Institute of Technology, Stockholm, Sweden
[b] Department of Chemical Engineering, KTH Royal Institute of Technology, Stockholm, Sweden
[c] Department of Mechanical Engineering, Chalmers University of Technology, Göteborg, Sweden

ARTICLE INFO

Keywords:
Carbon fiber
Multifunctional
Structural
Energy storage
Shape-morphing
Sensing
Energy harvesting

ABSTRACT

In nature, almost all materials perform multiple functions simultaneously, whereas man-made materials are typically optimized for a single function. Multifunctional materials offer a pathway to mimic nature, enabling materials that require fewer resources, reduce system mass and volume, and improve energy efficiency. Although multifunctional materials exist, they rarely combine more than two functions at the same time. Here we demonstrate a carbon fiber (CF) composite material that exhibits five different physical functions simultaneously: structural load carrying, energy storage, strain sensing, shape-morphing, and energy harvesting. This is achieved by utilizing the mechanical properties of CFs, their ability to reversibly intercalate Li-ions in their atomic structure, and the piezo-electrochemical transducer effect observed in lithiated CFs. The composite provides flexible performance, as it can be tailored toward specific functions through the design of its constituent materials and architecture. This concept could lead to significantly more efficient structural materials for a wide range of future applications.

Introduction

The transition toward sustainable technologies is driving a growing demand for lightweight and energy efficient systems across various industries. This demand is particularly evident in the transportation sector, where the pursuit of electrification and carbon neutrality is paving the way for innovative designs [1].

Traditional designs usually rely on monofunctional materials or components, such as batteries, sensors, actuators, and structural reinforcements, each serving a single function and then combined into a system. While effective, this design approach adds mass and complexity, since each function constitutes a penalty in mass, and the additional connections and interfaces required to integrate them further complicate the system. As a result, the energy performance is compromised, making it more challenging to achieve sustainability goals. For example, current battery systems are designed for energy storage but require a casing to meet mechanical requirements, which not only adds material but also decreases the energy density of the battery system. Similarly, actuators typically depend on heavy mechanical motors or pumps, which introduce additional parasitic mass.

As an alternative to traditional designs based on monofunctional materials, multifunctional materials can be employed. By reducing the need for separate components and connectors, they can lower system mass and volume. Despite potential design and manufacturing challenges, these materials can offer more energy and resource efficient solutions. This approach is inspired by nature, where most biological materials are composites capable of performing a variety of functions [2].

Piezoelectric materials represent a well-established class of multifunctional materials. Due to their electromechanical coupling, they can be used as sensors, actuators, and energy harvesters [3,4]. However, they often require a high-voltage power supply and are inherently non-structural. Therefore, they are typically embedded in composite structures [5,6] or grown on reinforcing fibers [7] to add structural properties. Such composites perform optimally only at high frequencies, limiting their effectiveness for low-frequency applications.

From an energy storage perspective, significant efforts have been devoted to the development of multifunctional batteries that combine

* Corresponding author.
E-mail address: danz@kth.se (D. Zenkert).

https://doi.org/10.1016/j.mattod.2026.103422
Received 18 February 2026; Received in revised form 12 May 2026; Accepted 6 June 2026
Available online 11 June 2026

energy storage with additional functionalities [8]. One of the most widely explored concepts is the structural battery, i.e. a composite material that can simultaneously carry mechanical loads and store electrical energy [9]. However, many studies add the structural functionality by embedding a lithium-ion battery within a composite or by using carbon fibers as current collectors, without fully exploiting the electrochemical properties of the fibers [10–12]. A more promising approach is a structural battery in which carbon fibers both carry mechanical loads and function as active electrodes by leveraging their ability to intercalate lithium ions [13]. This approach has high potential, as it allows for direct energy storage within the composite material, thereby minimizing overall system mass.

Composite materials are, by definition, a combination of two or more materials, which makes them well-suited for integrating multiple functionalities. Traditional structural composites typically consist of reinforcing fibers that carry mechanical loads embedded in a polymer matrix that joins the fibers together and transfers loads between them. Among the reinforcing fibers, carbon fibers (CFs) are renowned for being electrically conductive and for their exceptional mechanical properties, such as high strength and stiffness to weight ratios, making them ideal for structural applications. More recently, their electrochemical properties have also attracted significant attention, as CFs can intercalate lithium ions into their structure and thereby act as negative electrodes in Li-ion batteries. In a structural battery, pristine CFs are used as the negative electrode while CFs coated with active cathode material can be used on the positive side [14–17]. The CFs also act as current collectors, eliminating the need for the electrodes to be covered by metallic sheets. Several factors influence the performance of a structural battery, but when it comes to selecting the matrix, the key parameters are ionic conductivity and mechanical load transfer between the fibers. To address these requirements, Schneider et al. have developed a bicontinuous polymer electrolyte system, referred to as a structural battery electrolyte (SBE) [18]. The SBE consists of a homogeneous liquid that upon polymerization converts into a heterogeneous material: a liquid phase provides ionic conductivity and a polymer matrix provides mechanical properties. Recent studies have shown that using such SBE's structural batteries can achieve energy densities of around 33 Wh kg^{-1} and an elastic modulus ranging from 38 to 76 GPa [19,20].

Upon ion insertion, CFs exhibit a reversible longitudinal expansion of up to 1% [21]. This phenomenon is usually regarded as an adverse effect for energy storage devices. However, it can be used to realize a shape-morphing composite using electrochemical actuation, i.e. by changing the concentration of the inserted species in the fibers [22]. The expansion in the fibers is maintained even when no current is running, a so called zero-power hold. Therefore, electrochemical actuation offers a lightweight and efficient alternative to conventional actuation methods, such as hydraulic or motor-driven systems, which are typically bulky and require a continuous power supply. However, electrochemical actuation devices are limited by low operating frequency, making them suitable for low-frequency applications.

Ionically charged CFs exhibit the piezo-electrochemical transducer (PECT) effect, which is a coupling between the mechanical strain and the electrical potential of the material [23], similar to a piezoelectric material. This phenomenon enables CFs to function as strain sensors and energy harvesters [24]. By deforming the laminate, a voltage difference is generated between the electrodes that can be used either to power an external load or to determine the mechanical strain of the fibers. PECT-based energy harvesting is limited to a low-frequency regime due to the ion diffusion process [25]. However, the materials in [22] and [24] required to be pre-charged externally and would eventually self-discharge, resulting in the loss of all functionalities aside from the structural one.

Despite the advancements in multifunctional materials, a persistent challenge remains in achieving a material that effectively integrates multiple functionalities while providing mechanical load bearing capabilities. Previous research has focused on examining the CF properties individually or in limited combinations, but the complete integration of these functionalities in a single device is yet to be realized. Building on the structural battery concept, we present a multifunctional carbon fiber composite laminate that by exploiting both the mechanical properties of carbon fibers and their electrochemical ability to intercalate lithium integrates five distinct functions—energy storage, strain sensing, shape morphing, energy harvesting, and structural reinforcement—within a single composite material.

The multifunctional composite lay-up presented here consists of one layer of CFs coated with lithium iron phosphate (LFP) sandwiched between two layers of unidirectional commercially available CFs. Two glass veil layers and two commercial ceramic separators per laminate are used between the coated and uncoated CF layers to avoid short-circuit. The laminate is infused through vacuum-assisted infusion with SBE and then cured.

The resulting structural composite can be electrochemically cycled as a conventional energy storage device, delivering an energy density of 15.7 Wh kg^{-1}, an elastic modulus of 34.8 GPa, and a tensile strength of 194.0 MPa. The lithium content in the upper and lower carbon fiber layers can be independently electrically controlled, allowing the laminate to morph in a bending motion and be used as an actuator. Additionally, it can serve as a strain sensor through the PECT effect and harvest energy by converting mechanical work into electrical power. Altogether, this work presents a single material that integrates five distinct physical functions, with all the electrochemical functions enabled through only one set of electrical connections. Moreover, the operational lifetime of the morphing, sensing, and harvesting functionalities is self-sustained, as the LFP can be used to periodically recharge the CFs.

Results and discussions

Design and manufacture of multifunctional composite laminate

The multifunctional laminate was fabricated with a symmetric layup. The layup consisted of two outer layers of pristine unidirectional CFs and one middle layer of LFP-coated CFs, with separators placed between the outer and central layers to prevent direct contact, as illustrated in Fig. 1a. The LFP was deposited on the CFs through electrophoretic deposition (EPD), which enables control of the LFP mass loading on the CFs by adjusting the deposition conditions [17]. The EPD process is performed on both sides of the CF spread tow. As a result, the LFP forms a dominant outer coating layer while also partially infiltrating between individual filaments, which is consistent with the EPD deposition mechanism (Fig. S1). A concentration gradient is observed from the exterior toward the interior of the tow due to filament packing and transport limitations. To provide electrical insulation, thin glass veil layers were placed at both the top and bottom of the laminate. All layers were arranged on a glass plate, sealed, and infused with SBE through vacuum-assisted infusion, then cured at 90 °C for 90 min (Fig. 1b).

A total of three identical laminates were fabricated following the procedures described above. Unless otherwise specified, the results presented in the following sections refer to one laminate, while the corresponding data for the remaining laminates are reported in the Supplementary Information. All types of tests described in this work were performed on each laminate.

The layer thicknesses were measured using optical microscopy on cross-sections of the laminates. For the representative laminate, the total thickness was approximately 439 μm, with an average thickness of 60 μm for the two pristine CF layers and 139 μm for the LFP-coated CF layer. The layer thicknesses for all laminates are summarized in Supplementary Table S1. A representative cross-section is shown in Fig. 1c, and a cross-section with layer measurements is provided in Fig. S2.

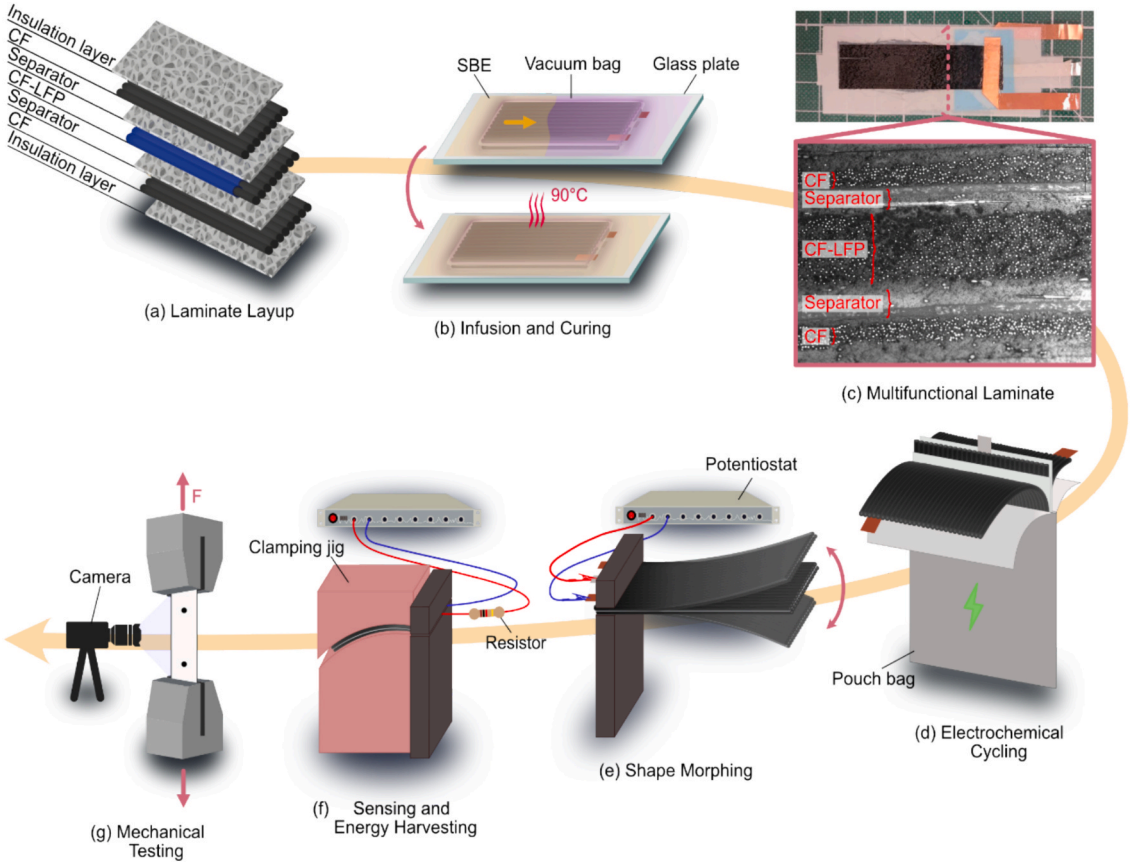

Fig. 1. Schematic illustration for the fabrication and the different functions of the multifunctional composite laminate. (a) Dry layup consisting of two outer layers of pristine unidirectional CFs, a central layer of LFP-coated CFs, and separators positioned between them. Glass veil layers are placed at both the top and bottom of the laminate to provide electrical insulation. (b) The layup is placed on a glass plate, sealed with vacuum sealing bag, infused with SBE and cured for 90 min at 90 °C. (c) Photograph showing the multifunctional laminate after infusion and a cross-section image captured with a light microscope. (d) The laminate is sealed in a pouch bag and electrochemically cycled. (e) The laminate is removed from the pouch bag and clamped on one end to form a cantilever. The pristine CFs layers are cycled individually using a potentiostat, which causes longitudinal expansions and contractions in the CFs due to lithiation and delithiation, allowing the laminate to morph in a bending deformation. (f) The clamped laminate is bent using a jig of known curvature, while the voltage and current changes between the pristine CF layers generated by the PECT effect are measured using a potentiostat under open-circuit and short-circuit conditions, respectively. A resistor can be connected in series to determine the power that can be harvested as the laminate is deformed. (g) The laminate is characterized mechanically using tensile testing. Longitudinal samples are painted white and marked with two surface markers to allow strain measurement via digital image correlation. For the transverse samples, no surface preparation is required, and the strain is recorded directly from the tensile tester.

Electrochemical performance

The fabricated multifunctional laminate was sealed inside a pouch bag (Fig. 1d) and was evaluated electrochemically in a full cell configuration consisting of LFP-coated CFs serving as the positive electrode (CF-LFP/PE) and pristine CFs as the negative electrodes (CF/NEs). The two CF/NE layers were connected to the same electrical connector to allow them to be cycled simultaneously. Galvanostatic cycling at

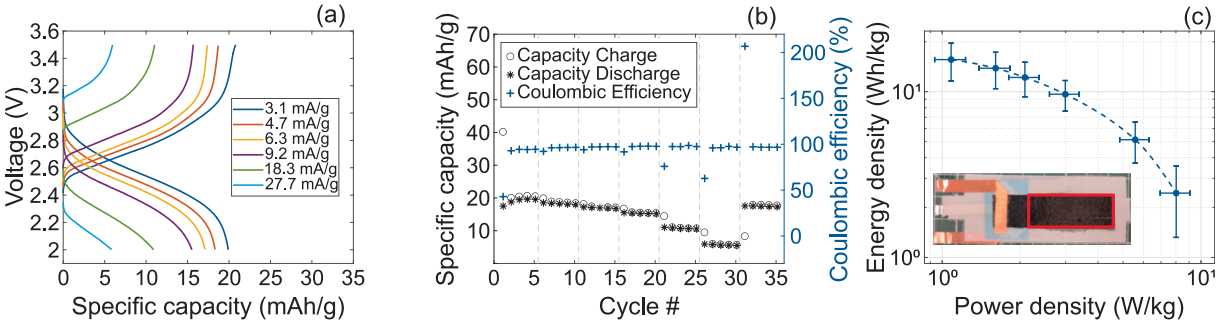

Fig. 2. Electrochemical testing of the multifunctional composite laminate. (a) Charge/discharge profile of the laminate for varying currents. (b) Specific capacity and coulombic efficiency with the following specific currents: 3.1, 4.7, 6.3, 9.2, 18.3, 27.7, and 3.1 mA g^{-1}. Each specific current was applied for 5 cycles. Specific currents relate to the mass of LFP in the positive electrode, whereas specific capacity relates to the total mass of active material (CF/NEs + LFP mass). Specific capacities calculated using either the CF/NEs mass or the LFP mass are reported in Supplementary Table S2. Results for all the laminates are shown in Fig. S3. (c) Ragone plot representing the discharge energy and power density relation of the multifunctional laminate based on the mass of the electrochemically active area highlighted in red. Data are presented as mean ± SD from all laminates.

various specific currents in the voltage range of 2 V to 3.5 V was used to assess the rate performance.

The charge–discharge profiles of the multifunctional laminate at different specific currents are presented in Fig. 2a. The maximum specific capacity achieved is approximately 20mAh g^{-1}, normalized by the total mass of active material, which is comparable to values reported in a previous study for CF structural batteries [20]. It is interesting to note that the profile curves exhibit a sharp increase/decrease towards the end of the charge/discharge, especially for lower currents. Since such a sharp increase/decrease in voltage is characteristic for a low/high state of lithiation of the LFP, this shows that the LFP is in fact limiting the capacity at low specific currents. This was anticipated, as the mass loading of LFP employed in this study (~8 mg cm^{-2}) is insufficient to fully charge both CF/NEs at the same time. The theoretical capacity of LFP is approximately 170mAh g^{-1}, while the capacity of CF has been experimentally measured to be around 250mAh g^{-1} [26,27]. The combined areal mass of the two CF/NEs is approximately 6.8 mg cm^{-2}, therefore the available LFP in the positive electrode is enough to fully charge one CF/NE, but not both. Based on the areal mass and specific capacities of both CF/NEs and CF-LFP/PE the theoretical LFP mass loading required for perfect capacity matching is approximately 10 mg cm^{-2}. Initial fabrication attempts targeted this value, after which the LFP mass loading was gradually reduced. This choice offers two advantages. First, using less LFP increases the volume fraction of CF, thereby improving the mechanical properties of the laminate. Second, increasing the thickness of the CF-LFP/PE lengthens the diffusion path for lithium ions, especially for those located deep within the electrode, farthest from the outer CF/NEs. This extended path can introduce diffusion limitations, reducing the amount of lithium that can be effectively utilized. Any lithium rendered inaccessible by these limitations becomes inactive mass within the cell, thereby lowering its overall energy density.

At a mass loading of ~ 8 mg cm^{-2}, only a modest decrease in maximum capacity was observed, while the rate performance improved significantly at higher current densities (Fig. S4). Therefore, this mass loading was selected as a compromise between energy density and rate capability. Further reducing the LFP mass loading would provide additional improvements in rate performance and mechanical properties, but at the expense of the maximum energy density that can be stored in the laminate.

Fig. 2b provides a more detailed view of the electrochemical behavior of the multifunctional laminate, showing the specific capacity and coulombic efficiency for each cycle. As expected, the specific capacity decreases as the current is increased; however, the rate performance test reveals that this decrease is reversible, as the initial capacity is regained in the final five cycles, when the lowest current is applied again. After stabilizing during the first few cycles, the multifunctional laminate operates at a coulombic efficiency over 98%. Coulombic efficiency is an important metric of the system's reversibility, and the initial coulombic efficiency is approximately 50% for all the cells. Irreversible loss of lithium, causing a lower initial coulombic efficiency, is a known phenomenon for lithium-ion batteries and is primarily attributed to lithium consumption associated with the formation of the solid–electrolyte interphase (SEI) layer, which is a passivation layer that is formed at the interface between the negative electrode and the electrolyte, by decomposition products of the electrolyte [28]. In structural batteries, an additional contribution arises from lithium irreversibly trapped within the carbon fiber microstructure during the first charge [29]. Notably, in cycle #31, the coulombic efficiency exceeds 100%. This behavior results from the transition from a higher to a lower specific current. During cycle #30, the discharge at the higher current experiences larger overpotentials, preventing full lithiation of the limiting CF-LFP/PE. Consequently, the subsequent charge at the lower current only transfers the lithium already present in the LFP electrode to the CF/NE. The following discharge at the same lower current (cycle #31), which is less affected by overpotentials, then accesses all the lithium in the CF/NE and transfers it back to the LFP electrode. The reverse occurs when shifting from a lower to a higher specific current, leading to an initially reduced coulombic efficiency (cycles #6, 11, 16, 21, and 26).

Finally, the energy and power density performance of the multifunctional laminate is illustrated in the Ragone plot in Fig. 2c. The energy and power densities considered here refer to the total mass of the active electrochemical area highlighted in red in Fig. 2c; this includes the CF-LFP/PE, the two CF/NEs, the separators, the insulation layers, and the SBE. The multifunctional laminate can achieve a discharge energy density that ranges from 15.7 Wh kg^{-1} to 2.5 Wh kg^{-1}, while the power density ranges from 1.1 W kg^{-1} to 8.1 W kg^{-1}.

These values are lower than those reported in the literature for CF structural batteries [19,20]. This is because the total mass considered in this work includes the insulation layers, which increases the overall mass, and because the LFP is the limiting electrode, as explained previously. At lower currents, the energy remains nearly constant while the power increases. This behavior is also evident in the rate performance test, where the capacity shows little variation as the current is increased. Such performance can be attributed to the low resistance in the laminates, which was measured using electrochemical impedance spectroscopy (EIS) between the two CF/NEs and found to be approximately 430 Ω (Fig. S5).

Shape morphing capability

Taking advantage of the reversible longitudinal expansion of the CF/NEs when inserted with lithium, the multifunctional laminate could be morphed in shape using electrochemistry (Fig. 1e). In the laminate architecture, the CF/NEs are placed on the outside, which maximizes the laminate's blocking force, defined as the maximum force that can be generated by an actuator, corresponding to the tip force required to produce a zero tip displacement.

Morphing experiments were conducted inside an argon-filled glovebox, where the laminate was removed from its pouch bag, wrapped in a thin layer of low-density polyethylene to prevent the liquid phase of the SBE from evaporating, and clamped on one end to form a cantilever. Subsequently, galvanostatic charge/discharge between 2 V and 3.5 V was performed on each CF/NE individually, first at 3.1 mA g^{-1} and then at 4.6 mA g^{-1}, starting from both CF/NE fully discharged. Cycling a single CF/NE at a time caused only that layer to undergo longitudinal expansion due to lithium insertion, while the other electrode remained unchanged. This difference in mechanical strain generated a bending deformation in the laminate in one direction. Repeating the procedure on the other CF/NE induced bending in the opposite direction. Following the charging of each CF/NE, a 30 min relaxation period without current was applied, during which the deformation persisted, confirming the multifunctional laminate's zero-power hold capability. Fig. 3a highlights the maximum upward and downward deformations of the laminate for the lower current. The experiment was recorded as a time-lapse using a camera and is provided in Supplementary Video 1.

In addition to the experimental observations, an analytical model based on classical laminate theory was used to predict the bending behavior of the multifunctional laminate. In the model, fiber expansion due to lithiation was represented through an analogy to thermal expansion, where the temperature change was replaced by the change in charge and the expansion coefficient $\beta = 2.6x10^{-5}$ g $mA^{-1}h^{-1}$ was used. The model has been previously validated for a similar setup [22], and the complete set of input parameters used in this work is provided in Supplementary Table S3.

A comparison between the analytical model output and the experimental data is shown in Fig. 3b, where the specific change in charge, relative only to the mass of the CF/NE that is cycled, is plotted against the laminate tip displacement. The experimental tip displacement values were obtained from the time-lapse recordings using the graph paper placed behind the sample. Pictures of the laminate at various stages, corresponding to different capacities, are also shown, demonstrating

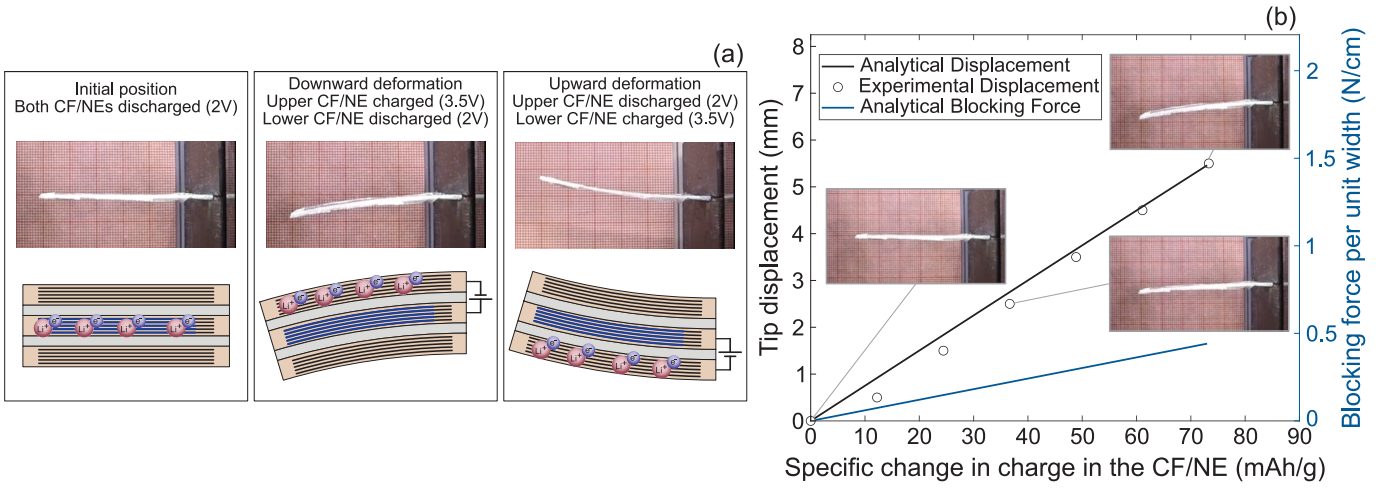

Fig. 3. Morphing experiment. (a) The experiment begins with both CF/NEs being discharged to 2 V. The upper CF/NE is then charged to 3.5 V, driving Li-ions from the CF-LFP/PE to the CF/NE. The charging of the CF/NE causes it to expand in the fiber direction, generating a downward bending deformation. The same procedure is repeated for the lower CF/NE, creating an upward bending deformation. A vertical tip displacement of 5.5 mm is achieved in both bending directions for a cantilever length of 45 mm and a specific change of charge in each CF/NE of around 70mAh g^{-1}, reached over approximately 10 h. (b) Comparison between experiment and analytical prediction of vertical tip displacement vs specific change in charge in the CF/NE that is cycled. Analytical predictions of the blocking force per unit width are also included.

that the model captures the bending behavior. Moreover, the blocking force is also plotted and expressed per unit width. A summary of the experimental and predicted morphing performance for all laminates is provided in Supplementary Table S4.

From Fig. 3b, it is evident that the analytical model accurately captures the behavior of the laminate. Moreover, the model can be used to evaluate the force that can be generated and can be adapted to other laminate layups, provided that the properties of each constituent layer are known.

The morphing experiment was carried out by charging each CF/NE individually, using half of two specific currents previously applied during the rate performance test, specifically 6.3 and 9.2 mA g^{-1}. In the earlier test, both CF/NEs were cycled simultaneously, whereas in this experiment, only one layer was used at a time. Using half of the specific currents ensured that each CF/NE experienced the same current in both experiments. Under these conditions, the expected capacity would normally be half of that obtained when both CF/NEs were cycled together. However, during the rate performance test, the CF-LFP/PE was the limiting electrode because both CF/NEs were cycled simultaneously and shared the same positive electrode. When the CF/NEs were cycled individually, each one had access to the full positive electrode. As a result, during the morphing experiment, the CF/NEs became the limiting electrodes, and the measured capacity exceeded half of the value obtained during the electrochemical characterization.

Interestingly, when the laminate was morphed using the higher current, which corresponded to cycling the CF at almost twice the rate of the lower one, the resulting tip displacement remained nearly unchanged, further confirming the good rate performance of the laminate (see Supplementary Video 1).

The actuation kinetics are directly coupled to the electrochemical cycling behavior. Since the morphing originates from lithium insertion/extraction in the CFs, the mechanical response is expected to occur concurrently with lithiation/delithiation, and any response time would therefore be governed by the rate limiting electrochemical process. The deformation was found to be mechanically reversible, with the laminate returning to its initial flat state upon each discharge. No measurable charge–strain hysteresis was observed.

Strain sensing functionality

In addition to energy storage and shape morphing, the multifunctional laminate could exploit the PECT effect observed in lithiated CFs to act as a strain sensor. To enhance this sensing response, the CF/NE layers were placed on the outside of the layup, where the mechanical strains are the largest. The sensing response of the laminate was characterized by measuring the open-circuit voltage (OCV) and the short-circuit current (SCC) between the two CF/NEs as the laminate was subjected to controlled bending [24,25]. The OCV refers to the voltage difference between the electrodes under zero-current conditions, while the SCC denotes the current flowing between the electrodes when a zero voltage is applied. Experiments were performed in the glovebox, with both CF/NEs charged to around 50% state of charge, where the coupling between OCV and mechanical strain was previously observed to be at its peak [30]. Before testing, the CF/NEs were held in short circuit overnight to equalize any voltage difference between them. The laminate was mounted in the cantilever setup used for the morphing experiment, and mechanical deformations were applied using 3D-printed clamping jigs with a known curvature (Fig. 1f). The experimental protocol consisted of a downward deflection held for 15 s, followed by a 15 s relaxation period in the undeformed state, and then an upward deflection also held for 15 s. This sequence was repeated three times for each curvature.

Mechanical strain in each CF/NE was calculated using laminate theory. Since the strain varies linearly through the thickness during bending but is constant along the length of the cantilever, the average values within each layer were considered. Two different jigs were employed, corresponding to an average longitudinal strain $|\Delta\varepsilon|$ in each CF/NE of 0.13% and 0.17%. Bending the laminate ensures that both CF/NEs experience the same magnitude of strain, although one layer is in tension and the other in compression, resulting in a strain difference of $2|\Delta\varepsilon|$. Because the PECT response is equal in magnitude but opposite in sign for tension versus compression, measuring the response between the two CF/NEs effectively doubles the signal compared to measuring it between one CF/NE and the CF-LFP/PE (see Fig. S6).

The OCV was measured as the laminate was bent by imposing a zero current condition between the CF/NEs using a potentiostat. Subsequently, the SCC was measured by imposing a zero voltage between the electrodes. Both voltage and current signals were smoothed using a moving average with a window size of 10.

Fig. 4 shows the OCV and SCC responses of the laminate as strain is applied. Both responses increase with increasing strain, reaching maximum values of 1.93 ± 0.02 mV and 3.97 ± 0.27 μA, respectively,

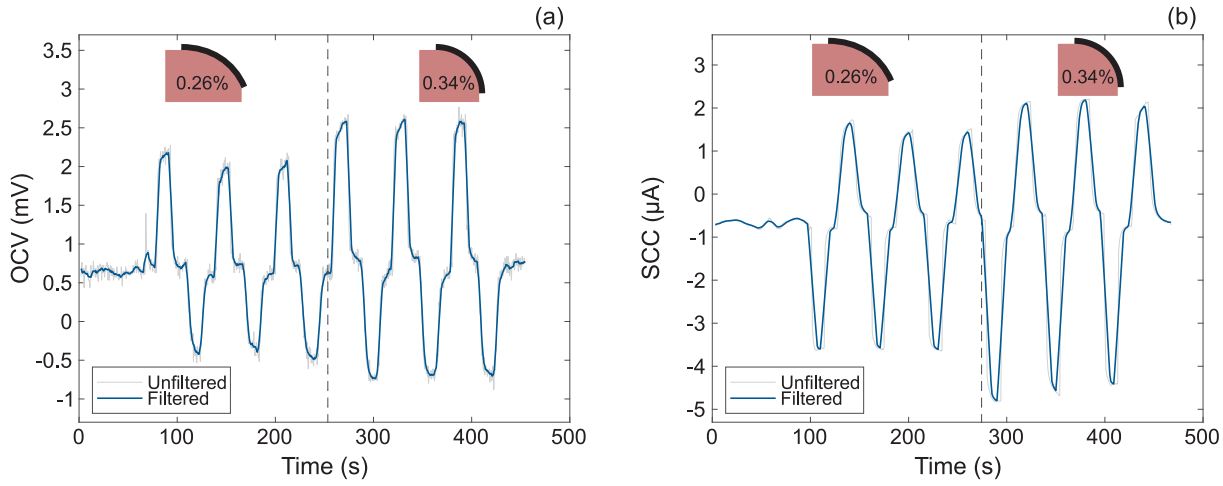

Fig. 4. PECT measurement. (a) OCV and (b) SCC between the two CF/NEs as a relative strain difference between them of 0.26% and 0.34%, is applied. The laminate is subjected to both upward and downward bending. Results for all the laminates are shown in Fig. S7.

for a downward deformation corresponding to a strain difference of 0.34% between the CF/NE layers. When the direction of deformation is reversed, the signs of both responses also reverse; although minor variations in magnitude are observed, the responses remain largely the same. Videos of the experiments are also provided in Supplementary Videos 2 and 3.

The response is not expected to originate from interfacial, volume changing or piezoresistive effects. Similar PECT behavior has previously been reported in liquid electrolyte systems [23], suggesting that CF/SBE interfacial effects are not responsible for the signal. Furthermore, the OCV measurements are performed under zero current conditions, meaning no Li-induced volume changes occur during deformation. Although a small current flows during SCC and energy harvesting measurements, the associated state of charge change is negligible due to the very low current and short deformation time. The estimated strain induced resistance variation of the CFs is also negligible compared to the total laminate resistance [31].

Energy harvesting performance

The PECT effect induces a change in OCV upon deformation when the CF/NEs are in open-circuit, or a change in SCC when they are in short-circuit. However, under these conditions, no actual power is generated, as either the current or the voltage is zero. Nevertheless, the product of these two values can still be used to estimate the theoretical maximum power that could be harvested. To determine the real power output, external electrical loads must be connected to the laminate, ensuring that both voltage and current are nonzero. According to the maximum power transfer theorem, the maximum power is delivered when the resistance of the external load matches the internal resistance of the laminate [32]. The resistance between the two CF/NEs was measured to be approximately 430 Ω using EIS (Fig. S5).

To characterize the energy harvesting ability of the multifunctional laminate, the procedure described by Preimesberger et al. was followed [33]. Resistors of 56, 180, 390, 820, and 1800 Ω were individually connected in series to the laminate, which was then subjected to bending using the jig introduced in the previous section, corresponding to a relative strain difference between the CF/NEs of $2|\Delta\varepsilon| = 0.34\%$ in each CF/NE (Fig. 1f). The CF/NEs were short-circuited, and the SCC was measured. As expected, the measured current response decreased with increasing resistance, as shown in Fig. 5a. The current change was then used to calculate the voltage across the external resistor using Ohm's law, and the power was determined as the product of the current and voltage. The power output versus the voltage change during deformation for the different resistors is shown in Fig. 5b.

The maximum experimentally measured power from the

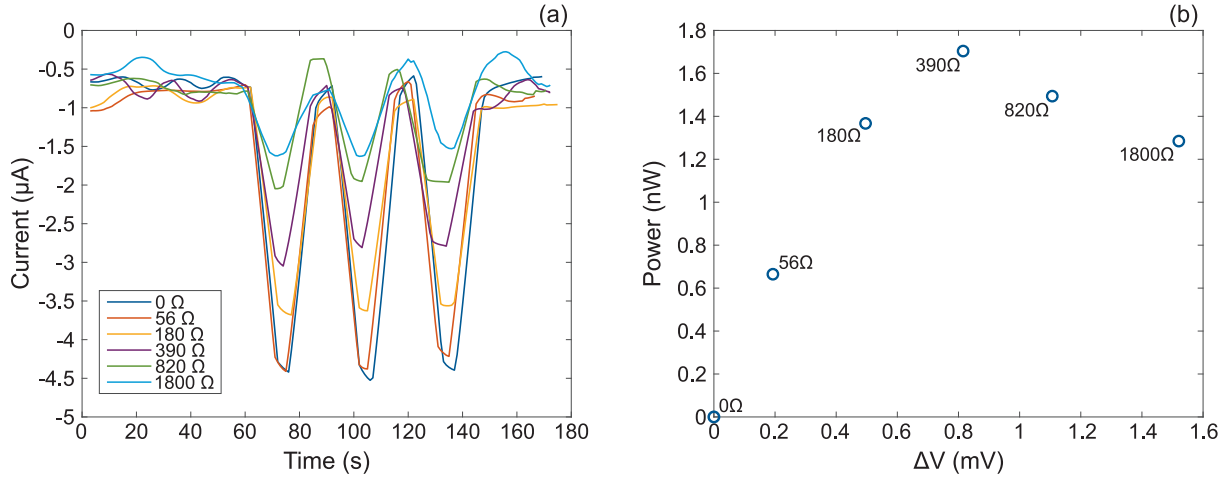

Fig. 5. Energy harvesting results. (a) SCC response between the CF/NEs as a relative strain difference between them of 0.34% is applied. The experiment is repeated for different external resistive loads connected in series to the laminate. (b) Power profile of the multifunctional laminate across different resistive loads. Results for all the laminates are shown in Fig. S8.

multifunctional laminate is 1.7 nW, compared with a theoretical power of approximately 7.7 nW. The fill factor, defined as the ratio of measured maximum power to theoretical maximum power, provides a useful metric for evaluating the performance of the PECT energy harvester and is around 22%. This metric is commonly used in the evaluation of photovoltaic systems and is adapted here for energy harvesting characterization. The maximum power is obtained using a 390 Ω external resistor, which closely matches the laminate's internal resistance. This observation is consistent with the maximum power transfer theorem.

It should be noted that the power value reported in this study corresponds to an average relative strain difference between the CF/NEs of 0.34%. Because the harvested power scales with the square of the applied strain, higher power outputs can be achieved by increasing the strain, provided the mechanical integrity of the laminate is maintained and no failure occurs. In contrast, the loading rate is expected to have only a minor influence on the harvested energy compared to the strain amplitude itself. The deformation in the present study was applied manually due to limitations of the experimental setup, resulting in limited control over the loading frequency. At higher frequencies, the system is expected to remain functional and based on the time constants linked to the electrochemical processes, frequencies above 1 Hz should still be possible to utilize for energy harvesting. However, at sufficiently high frequencies, lithiation/delithiation would likely no longer occur, and the response would instead become dominated by double-layer charging and discharging.

Mechanical characterization

After evaluating all the electrochemical functions, tensile tests were performed on the same laminates to assess their mechanical performance (Fig. 1g). Prior to testing, the laminates were dried to eliminate the liquid part of the SBE and sectioned into smaller testing samples oriented along both the longitudinal and transverse directions (Fig. S9). An example of a stress–strain profile from tensile testing for both directions is shown in Fig. S10.

The elastic moduli for both longitudinal and transverse directions were determined from the linear region of the stress–strain curves. The multifunctional laminates exhibit a longitudinal elastic modulus of 34.8 ± 3.4 GPa and a transverse elastic modulus of 944.0 ± 317.0 MPa. The maximum tensile strength was measured as 194.0 ± 35.9 MPa and 12.3 ± 5.7 MPa in the longitudinal and transverse directions, respectively.

The longitudinal mechanical properties are predominantly dependent on the fibers properties and their volume fraction, and they are reportedly known to be independent of the electrochemical cycling [19]. In contrast, the transverse properties are matrix dominated and usually decrease slightly after cycling [19]. This reduction can be attributed to the fact that CFs undergo radial expansion of up to 13% when fully lithiated [21], which can induce microdamage in the SBE and potentially compromise its mechanical integrity over time.

The longitudinal stiffness measured in this work is within the range reported for CF structural batteries, although on the lower side [19,20]. This reduction is expected, as the multifunctional laminate includes separators with two layers (glass veil and Freudenberg separator) as well as additional insulation layers, all of which reduce the overall fiber volume fraction and thus the stiffness. Importantly, the experimental results are consistent with the predictions of the analytical model, confirming that measured values align with the laminate layup.

Multifunctionality of the composite material

The laminate layup plays a critical role in enabling multifunctionality. Alternative layups, such as placing a CF/NE layer in the middle with two CF–LFP/PE layers on the outer surfaces, would preclude energy harvesting, strain sensing, and shape morphing. In contrast, the design presented here supports all of these functions, although it was not optimized to maximize any single one. However, depending on the application, the performance of the laminate can be tuned to favor certain functionalities over others. For example, decreasing the LFP mass loading would reduce the energy density, but it would enhance the mechanical stiffness due to the corresponding increase in fiber volume fraction, and a thinner LFP coating would also improve the laminate's morphing capability. Similarly, the SBE used in this work consists of 50% liquid electrolyte and 50% monomer. Increasing the liquid electrolyte content would improve the electrochemical performance at the expense of mechanical properties, whereas a higher monomer content would have the opposite effect. Moreover, changing the fiber orientation would enable additional morphing deformation modes, such as twisting [34], adding another degree of freedom to the laminate response. These trade-offs highlight the strong coupling among the five integrated functions, resulting in a five-dimensional design space that enables optimization of the laminate for a wide range of applications.

While all five functionalities are demonstrated using the same specimen, they were characterized individually in order to isolate and quantify each response. Indeed, several functions can operate simultaneously, for example, the laminate can store energy while being mechanically loaded and simultaneously perform strain sensing through changes in potential. However, standardized methodologies for simultaneous multifunctional characterization remain an open challenge [35].

The present work relies on off-the-shelf constituents from both batteries and composites, combined with scalable processing techniques such as EPD and vacuum-assisted infusion. However, the fabrication process used in this work inevitably introduces high variability in the performance. Variations in fiber spreading and local layer thickness influence the performance of all the functionalities. This highlights the need for more automated and high-precision manufacturing methods capable of ensuring consistent layer thickness and controlled fiber orientation throughout the laminate. Future developments such as multifunctional prepregs, 3D printing, and CFs tailored for both structural and electrochemical performance could further improve scalability, reproducibility, and overall performance [36,37].

Conclusion

This study serves as a proof-of-concept for a lightweight and resource-efficient multifunctional composite laminate capable of storing and harvesting energy, morphing its shape, functioning as a strain sensor, and carrying mechanical loads. The laminate delivers an energy density of 15.7 Wh kg^{-1} and a power density of up to 8.1 W kg^{-1}, it can harvest 1.7 nW for a change in strain in the CF/NE of 0.17, all while preserving a stiffness of 34.8 GPa. Shape morphing is electrically controlled at low voltage and provides a zero-power hold of the deformed configuration. Strain sensing is enabled by the PECT effect and provides continuous measurement without the need for external sensors. Remarkably, all five functions are enabled through only a set of electrical connections, underscoring the potential of this approach for highly integrated, mass-efficient structural systems.

Materials and methods

Materials

Intermediate modulus PAN-based T800SC-12 K-50C carbon fibers (CFs) with a linear density of ~ 5.2 mg cm^{-1} were manufactured by Toray Composite Materials America, Inc. and spread by Oxeon AB to a width of approximately 15 mm. $LiFePO_4$ powder (LFP; purity: 99.9%, APS: 80–100 nm) was purchased from Nanoshel UK, Ltd. Reduced graphene oxide (rGO) containing 95% carbon was obtained from LayerOne AS. Conductive Super P carbon black (CB, ~40 nm) and polydiallyldimethylammonium chloride (PDDA; 20 wt% in H_2O) were acquired from Thermo Scientific and Sigma Aldrich, respectively.

Freudenberg Performance Materials supplied the 23 μm-thick Freudenberg separator (FS-3002–23) with an areal mass of 33 g m^{-2}, while Technical Fibre Products Ltd. provided the fine E-glass fiber veil (Optiveil 20153B) with an areal mass of 6 g m^{-2}. The structural battery electrolyte (SBE) consisted of bisphenol A ethoxylate dimethacrylate (BPAMA) from Sartomer Company, Europe, 2–2′-azobis(2-methylpropionitrile) (AIBN) provided by Sigma-Aldrich, and 1 M lithium bis (trifluoromethanesulfonyl)imide (LiTFSI) in a 50:50 wt% mixture of ethylene carbonate (EC) and propylene carbonate (PC) with a purity of 99.9% supplied by Solvionic and used as received. Copper foil (17 μm, 99.95% purity) and aluminium foil (25 μm, 99.2% purity) current collectors were purchased from Advent Research Material Ltd.. The silver conductive paint SCP03B from Electrolube and the thermoset conductive ink XZ302-1 (Sunchemical) supplied by Tronti Oy were used to attach the current collectors to the CFs. PET/Al/PE (12 μm/9 μm/75 μm) from Skultuna Flexible was used as pouch material.

Preparation of structural electrodes

The CFs were desized by refluxing them in dichloromethane for 12 h to remove the polymer coating, after which they served as the substrate for electrophoretic deposition (EPD) of the positive electrode. EPD was performed at room temperature in a two-electrode setup using a Keithley 2450 SourceMeter to apply a constant 80 V, with the fibers (50 mm × 15 mm immersed area) acting as the working electrode and a platinum-coated titanium mesh placed 15 mm away as the counter electrode. The deposition suspension was prepared by sonicating LFP (500 mg in 50 mL ethanol) for 20 min, then adding rGO and CB (50 mg each) as conductive additives, dispersed separately in ethanol. A small amount of the cationic polymer PDDA (500 μL in ethanol) was introduced to positively charge the suspension, followed by an additional sonication step. The final mixture comprising of 90 wt% LFP and 5 wt% each of rGO and CB was used for a 10-minute cathodic deposition onto fibers spread to a width of 15 mm. After coating, the samples were dried at 70 °C and cut to a total length of 50 mm. Aluminium current collectors were then attached to the uncoated region using the thermoset conductive ink and cured at 150 °C for 2 h, completing the preparation of the LFP-coated CFs that served as the positive electrode (CF-LFP/PE).

For the preparation of the CF negative electrodes (CF/NEs), two additional layers of pristine CFs were cut to around 60 mm. Copper current collectors were then attached to one end of each layer using silver conductive paint and dried in ambient conditions.

Manufacturing of multifunctional composite laminate

The manufacturing of the composite laminate was made by stacking of dry layers on a glass plate. The stacking sequence was symmetric, beginning with the CF/NE, followed by the Freudenberg separator and the glass veil. At the center of the stack, the CF-LFP/PE was placed. The sequence was then mirrored, with another glass veil, a Freudenberg separator, and a layer of CF/NE. As a result, the electrochemically active area had a length of approximately 45 mm. Additionally, a layer of glass veil was positioned at the top and bottom of the stack to provide electrical insulation for the laminate. The stack was sealed with vacuum sealing bag and vacuum-dried for 12 h at 60 °C.

The SBE was prepared inside a glovebox in argon atmosphere and dry conditions (<1 ppm of H_2O, <4 ppm of O_2) by mixing 49.75 wt% BPAMA, 0.50 wt% AIBN and 49.75 wt% liquid electrolyte (1 M LiTFSI in EC:PC 50:50 wt%) and then stirred using a vortex mixer to obtain a homogeneous mixture. The SBE was used to vacuum-infuse the dry layups and cured in an oven for 90 min at 90 °C.

The cured laminates were demoulded inside the glovebox, and 100 μL of liquid electrolyte was added on each side before the laminates were vacuum-sealed in pouch bags.

Electrochemical characterization

Galvanostatic cycling was conducted using a Neware battery cycler (BTS5V100mA8CH) within a voltage range of 2–3.5 V with the LFP-coated CFs serving as the positive electrode and pristine CFs as the negative electrode. The two CF/NEs were connected to the same electrical connector to ensure simultaneous cycling.

The cycling protocol comprised five charge/discharge cycles at each of the following specific currents: 3.1, 4.7, 6.3, 9.2, 18.3, and 27.7 mA g^{-1}, followed by an additional five cycles at 3.1 mA g^{-1} to conclude the test. The currents were normalized by the mass of LFP.

Electrochemical Impedance Spectroscopy (EIS) was performed on a VMP3 Biologic potentiostat between the two CF/NEs between 0.1 Hz and 100 kHz with an AC amplitude of 10 mV. Before EIS, the laminates were charged to 50% state of charge.

Morphing experiment setup

Following electrochemical cycling, the pouch cell was opened in an argon-filled glovebox, and the laminate was wrapped in a 15 μm thick low-density polyethylene film. The laminate was then mounted in a custom test rig, where one end was clamped to establish a cantilever setup. The aluminium current collector and one copper current collector at a time were connected to a Biologic SP-50 potentiostat used for galvanostatic cycling, which was performed first at a specific current of 3.1 mA g^{-1} and then at 4.6 mA g^{-1}. The experiment began with both CF/NEs fully discharged. The morphing protocol involved charging one CF/NE to 3.5 V, followed by a relaxation period of 30 min where no current was applied, and then discharging it to 2 V. This sequence was used for both currents and subsequently repeated on the second CF/NE. The vertical tip deflections were measured from the time-lapse video obtained using a GoPro Hero4 Session camera.

Strain sensing measurements

The same setup used for the morphing experiment was used for this test. Before testing, the top and bottom CF/NEs were connected together and charged to approximately 50% of the total capacity using a specific current of 3.1 mA g^{-1}. To equalize the voltage between the CF/NEs, they were subsequently held in short circuit overnight. For the experiment, 3D-printed clamping jigs with curvatures of 120 mm and 90 mm were used to deform the laminate along the fiber direction. The deformation protocol consisted of bending the laminate into the jig's curvature in one direction and holding it for 15 s, followed by a 15-second relaxation period in the undeformed state. The laminate was then bent in the opposite direction using the same hold and relaxation durations. This procedure was repeated three times for each curvature. Electrochemical measurements were taken throughout the mechanical cycling using a Biologic SP-50 potentiostat. First, the open-circuit voltage (OCV) was measured between one of the CF/NE and the CF-LFP/PE. Then the same was done with the second CF/NE. Finally, two more mechanical cycles were performed to measure the OCV and the short-circuit current (SCC) between the two CF/NEs. The experiment was recorded using a GoPro Hero4 Session camera.

Energy harvesting measurements

The experimental setup previously described was retained for this set of measurements. Similarly to the sensing experiment, the CF/NEs were short circuited to eliminate any voltage difference. Following this, different resistors were individually connected in series to the laminate. Mechanical deformation was applied using the 3D-printed jig with the 90 mm curvature, where the laminate was bent three times in one direction, with each bend held for 15 s, followed by a 15-second relaxation period. During deformation, the Biologic SP-50 potentiostat maintained a zero-voltage condition between the two CF/NEs, while the current was

recorded. The voltage change across the resistors was calculated according to Ohm's law, and the output power was then determined by multiplying the voltage change by the corresponding current.

Mechanical testing

Before mechanical testing, the laminates were dried on a heating plate at 60 °C for 12 h to remove the liquid part of the SBE. The laminates were then cut into smaller testing samples, measuring 25 mm × 4 mm along the fiber direction and 15 mm x 5 mm along the transverse direction. For each laminate, three samples were obtained in each direction.

For the measurements in the transverse direction, an ElectroForce DMA 3200 in tensile mode with a 500 N load cell was used for tensile testing. The samples were mounted directly on the grips of the machine and tested using a displacement rate of 0.3 mm min^{-1}.

For the tests in the longitudinal direction, glass fiber tabs were bonded to both ends of each specimen using an epoxy adhesive, resulting in a gauge length of 10 mm. One side of each sample was then painted white, and two circular markers were added on the surface. For the tensile testing, a Shimadzu Autograph AGS-X with a 5 kN load cell and a strain rate of 0.3 mm min^{-1} was used. The stress was recorded directly from the tensile tester while strain was measured by tracking the change in distance between the two markers using a GOM Aramis digital image correlation system.

The use of two different techniques ensured accurate measurements, as the DMA provided better precision for transverse testing, while the Shimadzu was better suited for longitudinal testing. The elastic modulus for both types of samples was calculated as the slope of the linear section of the resulting stress–strain curve.

Microscopy

Optical microscopy was performed on the dried laminates using an Olympus BX53M light microscope to measure the thickness of the individual layers. Cross-sections were prepared by cutting the laminates with a scalpel into smaller samples, which were subsequently fixed in a plastic holder, placed in a cup, and embedded in epoxy. A mixture of Qpox 90 hardener and Qpox 90 resin (ATM Qness GmbH) was used. The epoxy was allowed to cure for 24 h at ambient conditions, after which the surface was polished.

CRediT authorship contribution statement

Alfredo Bici: Writing – original draft, Visualization, Validation, Methodology, Data curation, Conceptualization. **Elvira Lind:** Writing – review & editing, Writing – original draft, Methodology, Investigation. **Richa Chaudhary:** Writing – review & editing, Writing – original draft, Methodology, Investigation. **Leif E. Asp:** Writing – review & editing, Supervision, Methodology, Funding acquisition. **Göran Lindbergh:** Writing – review & editing, Supervision, Methodology, Funding acquisition, Conceptualization. **Dan Zenkert:** Writing – review & editing, Supervision, Methodology, Funding acquisition, Conceptualization.

Declaration of competing interest

The authors declare that they have no known competing financial interests or personal relationships that could have appeared to influence the work reported in this paper.

Acknowledgements

This work was supported by the Swedish Energy Agency [project number 50508-1], the Swedish Research Council [project numbers 2021-05276 and 2024-04344], Air Force Office of Scientific Research [grant numbers FA8655-25-1-7047 and FA8655-25-1-7049], and 2DTECH VINNOVA Competence Centre [Ref. 2019-00068].

Appendix A. Supplementary data

Supplementary material includes additional figures, tables, and videos supporting the results of this study to this article can be found online at https://doi.org/10.1016/j.mattod.2026.103422.

Data availability

Data will be made available on request.

References

[1] P. Jaramillo, et al., Transport, in Climate Change 2022 - Mitigation of Climate Change, Cambridge University Press, 2023, pp1049–1160. https://doi.org/10.1017/9781009157926.012.
[2] K. Salonitis, et al., Multifunctional materials: engineering applications and processing challenges, Int. J. Adv. Manuf. Technol. 49 (2010) 803–826, https://doi.org/10.1007/s00170-009-2428-6.
[3] A.D.B.L. Ferreira, P.R.O. Nóvoa, A.T. Marques, Multifunctional material systems: a state-of-the-art review, Compos. Struct. 151 (2016) 3–35, https://doi.org/10.1016/j.compstruct.2016.01.028.
[4] M. Safaei, H.A. Sodano, S.R. Anton, A review of energy harvesting using piezoelectric materials: state-of-the-art a decade later (2008–2018), Smart Mater. Struct. 28 (2019) 113001, https://doi.org/10.1088/1361-665X/AB36E4.
[5] M. Lin, F.K. Chang, The manufacture of composite structures with a built-in network of piezoceramics, Compos. Sci. Technol. 62 (2002) 919–939, https://doi.org/10.1016/S0266-3538(02)00007-6.
[6] P. Portela, et al., Analysis of morphing, multi stable structures actuated by piezoelectric patches, Comput. Struct. 86 (2008) 347–356, https://doi.org/10.1016/j.compstruc.2007.01.032.
[7] M.H. Malakooti, et al., ZnO nanowire interfaces for high strength multifunctional composites with embedded energy harvesting, Energy Environ. Sci. 9 (2016) 634–643, https://doi.org/10.1039/C5EE03181H.
[8] Y. Huang, M. Zhu, Y. Huang, et al., Multifunctional energy storage and conversion devices, Adv. Mater. 28 (2016) 8344–8364, https://doi.org/10.1002/adma.201601928.
[9] J.F. Snyder, E.L. Wong, C.W. Hubbard, Evaluation of commercially available carbon fibers, fabrics, and papers for potential use in multifunctional energy storage applications, J. Electrochem. Soc. 156 (2009) A215, https://doi.org/10.1149/1.3065070.
[10] T. Pereira, et al., Embedding thin-film lithium energy cells in structural composites, Compos. Sci. Technol. 68 (2008) 1935–1941, https://doi.org/10.1016/j.compscitech.2008.02.019.
[11] K. Moyer, C. Meng, B. Marshall, et al., Carbon fiber reinforced structural lithium-ion battery composite: multifunctional power integration for CubeSats, Energy Storage Mater. 24 (2020) 676–681, https://doi.org/10.1016/j.ensm.2019.08.003.
[12] Z. Yang, Y. Mu, L.H. Acauan, et al., Understanding and recent advances on lithium structural batteries, Chem. Eng. J. 502 (2024) 157772, https://doi.org/10.1016/j.cej.2024.157772.
[13] L.E. Asp, et al., Structural battery composites: a review, Funct. Compos. Struct. 1 (2019) 042001, https://doi.org/10.1088/2631-6331/ab5571.
[14] M.H. Kjell, et al., PAN-based carbon fiber negative electrodes for structural lithium-ion batteries, J. Electrochem. Soc. 158 (2011) A1455, https://doi.org/10.1149/2.053112jes.
[15] L.E. Asp, K. Bouton, D. Carlstedt, et al., A structural battery and its multifunctional performance, Adv. Energy Sustain. Res. 2 (2021) 2000093, https://doi.org/10.1002/aesr.202000093.
[16] Y.D. Yücel, E. Adolfsson, H. Dykhoff, et al., Powder-impregnated carbon fibers with lithium iron phosphate as positive electrodes in structural batteries, Compos. Sci. Technol. 241 (2023) 110153, https://doi.org/10.1016/j.compscitech.2023.110153.
[17] R. Chaudhary, et al., Structural positive electrodes engineered for multifunctionality, Adv. Sci. 11 (2024) 2404012, https://doi.org/10.1002/advs.202404012.
[18] L.M. Schneider, et al., Bicontinuous electrolytes via thermally initiated polymerization for structural lithium ion batteries, ACS Appl. Energy Mater. 2 (2019) 4362–4369, https://doi.org/10.1021/acsaem.9B00563.
[19] K. Bouton, et al., A structural battery with carbon fibre electrodes balancing multifunctional performance, Compos. Sci. Technol. 256 (2024) 110728, https://doi.org/10.1016/j.compscitech.2024.110728.
[20] R. Chaudhary, et al., Unveiling the multifunctional carbon fiber structural battery, Adv. Mater. (2024), https://doi.org/10.1002/adma.202409725.
[21] E. Jacques, et al., Expansion of carbon fibres induced by lithium intercalation for structural electrode applications, Carbon 59 (2013) 246–254, https://doi.org/10.1016/j.carbon.2013.03.015.
[22] W. Johannisson, et al., Shape-morphing carbon fiber composite using electrochemical actuation, Proc. Natl. Acad. Sci. U. S. A. 117 (2020) 7658–7664, https://doi.org/10.1073/pnas.1921132117.

[23] E. Jacques, et al., Piezo-electrochemical effect in lithium-intercalated carbon fibres, Electrochem. Commun. 35 (2013) 65–67, https://doi.org/10.1016/j.elecom.2013.07.040.
[24] R. Harnden, et al., Multifunctional carbon fiber composites: a structural, energy harvesting, strain-sensing material, ACS Appl. Mater. Interfaces 14 (2022) 33871–33880, https://doi.org/10.1021/acsami.2c08375.
[25] S. Kim, S.J. Choi, K. Zhao, et al., Electrochemically driven mechanical energy harvesting, Nat. Commun. 7 (2016) 1–7, https://doi.org/10.1038/ncomms10146.
[26] S.Y. Chung, J.T. Bloking, Y.M. Chiang, Electronically conductive phospho-olivines as lithium storage electrodes, Nat. Mater. 1 (2002) 123–128, https://doi.org/10.1038/nmat732.
[27] G. Fredi, S. Jeschke, A. Boulaoued, et al., Graphitic microstructure and performance of carbon fibre Li-ion structural battery electrodes, Multifunct. Mater. 1 (2018) 015003, https://doi.org/10.1088/2399-7532/aab707.
[28] A. Wang, et al., Review on modeling of the anode solid electrolyte interphase (SEI) for lithium-ion batteries, NPJ Comput. Mater. 4 (2018) 1–26, https://doi.org/10.1038/s41524-018-0064-0.
[29] E. Jacques, M.H. Kjell, D. Zenkert, et al., Impact of electrochemical cycling on the tensile properties of carbon fibres for structural lithium-ion composite batteries, Compos. Sci. Technol. 72 (2012) 792–798, https://doi.org/10.1016/j.compscitech.2012.02.006.
[30] E. Jacques, et al., Piezo-electrochemical energy harvesting with lithium-intercalating carbon fibers, ACS Appl. Mater. Interfaces 7 (2015) 13898–13904, https://doi.org/10.1021/acsami.5b02585.
[31] Y. Yao, J. Luo, X. Duan, et al., On the piezoresistive behavior of carbon fibers - cantilever-based testing method and Maxwell-Garnett effective medium theory modeling, Carbon 141 (2019) 283–290, https://doi.org/10.1016/j.carbon.2018.09.043.
[32] M. Plonus, Electronics and communications for scientists and engineers, second ed., Butterworth-Heinemann, Oxford, 2020.
[33] J.I. Preimesberger, S.Y. Kang, C.B. Arnold, Figures of merit for piezoelectrochemical energy-harvesting systems, Joule 4 (2020) 1893–1906, https://doi.org/10.1016/j.joule.2020.07.019.
[34] F. Dionisi, R. Harnden, D. Zenkert, A model to analyse deformations and stresses in structural batteries due to electrode expansions, Compos. Struct. 179 (2017) 580–589, https://doi.org/10.1016/j.compstruct.2017.07.029.
[35] E.S. Greenhalgh, S. Nguyen, L.E. Asp, et al., Characterization and reporting protocols for structural power composites: a perspective, Adv. Energy Mater. (2025), https://doi.org/10.1002/aenm.202404702.
[36] A. Thakur, X. Dong, Printing with 3D continuous carbon fiber multifunctional composites via UV-assisted coextrusion deposition, Manuf. Lett. 24 (2020) 1–5, https://doi.org/10.1016/j.mfglet.2020.02.001.
[37] R. Tavano, J. Xu, C. Creighton, et al., Influence of carbonisation temperatures on multifunctional properties of carbon fibres for structural battery applications, Batteries Supercaps (2024), https://doi.org/10.1002/batt.202400110.